ISSN 0915-633X

INTERNATIONAL ATOMIC ENERGY AGENCY

SIXTEENTH IAEA FUSION ENERGY CONFERENCE

Montréal, Canada, 7-11 October 1996

IAEA-CN-64/D3-6

NATIONAL INSTITUTE FOR FUSION SCIENCE

Ballooning Modes in Heliotrons/Torsatrons

N. Nakajima, K. Ichiguchi, M. Okamoto and R.L. Dewar

(Received - Sep. 27, 1996)

NIFS-452 Sep. 1996

RESEARCH REPORT
NIFS Series

NAGOYA, JAPAN

INTERNATIONAL ATOMIC ENERGY AGENCY

SIXTEENTH IAEA FUSION ENERGY CONFERENCE

Montréal, Canada, 7–11 October 1996

IAEA-CN-64/ D3-6

BALLOONING MODES IN HELIOTRONS/TORSATRONS

N. NAKAJIMA, K. ICHIGUCHI, M. OKAMOTO
National Institute for Fusion Science, Nagoya, Japan

R. L. DEWAR
Plasma Research Laboratory, ANU, Canbera ACT 0200, Australia

keywords: ballooning, local shear, local curvature, heliotron, torsatron

BALLOONING MODES IN HELIOTRONS/TORSATRONS

ABSTRACT

The characteristics of the high-n ballooning modes and the corresponding β (= kinetic pressure/magnetic pressure) limit are discussed in a planar-axis $L = 2/M = 10$ heliotron/torsatron with a large Shafranov shift (L and M are the polarity and toroidal pitch number of helical coils, respectively). The exact incompressible high-n ballooning mode equation for three-dimensional equilibria is solved in the covering space (ψ, η, α) where ψ and α are the labels of the flux surface and the magnetic field line, respectively, and η is the coordinate along the magnetic field line ($-\infty < \eta < \infty$). In three-dimensional equilibria, the eigenvalue generally depends on α: $\omega^2 = \omega^2(\psi, \theta_k, \alpha)$ with θ_k the radial wave number. From the analyses of the local magnetic shear associated with the toroidal force balance, the physical mechanism is clarified why the high-n ballooning modes can be unstable even in the region with stellarator-like global magnetic shear. Such high-n modes have strong α-dependece of ω^2 for a peaked pressure profile giving Mercier stable equilibria. In contrast, a broad pressure profile allows high-n modes with weak α-dependence of ω^2. The relationship between the high-n and low-n ballooning modes and the related β limit are also considered through the α-dependence of ω^2.

1. INTRODUCTION

In currentless helical systems with a planar-axis, such as heliotron/torsatron devices, the global rotational transform ι of the vacuum magnetic field increases in the minor radius direction. Using a low-β approximation, Shafranov[1] speculated that if the global shear is stellarator-like, then high-n ballooning modes would not become unstable when the Mercier modes are stable. Using three-dimensional equilibria, Cooper *et al.*[2] found high-n ballooning modes in the stellarator-like global magnetic shear region of the ATF[3]; however, they did not give the physical mechanism. The spectrum of ballooning modes in general toroidal systems has been investigated by Dewar *et al.*[4] using a model tokamak with toroidal field ripples in order to study the affects of symmetry breaking on the ballooning spectrum. Recently, an examination similar to that in Ref. [4] was carried out for high-n ballooning modes in an LHD[5] equilibrium with a broad pressure profile, thus strongly Mercier-unstable[6]. In that work, a modified high-n ballooning equation is used, so that it was not clear how the kinetic energy norm affected the eigenvalues so obtained.

In this paper, we will investigate the stability properties of ballooning modes, both in strongly Mercier-unstable and completely Mercier-stable equilibria, for an $L = 2/M = 10$ heliotron/torsatron system with a large Shafranov shift, with the use of the exact incompressible three-dimensional high-n ballooning mode equation[7].

2. GLOBAL EQUILIBRIUM CHARACTERISTICS

For the vacuum configuration, we will use the planar-axis $L = 2/M = 10$ heliotron/torsatron configuration. Only currentless equilibria will be calculated with the use of the VMEC code[8] for fixed boundary conditions, with the boundary determined as the outermost flux surface of the vacuum field. Two types of pressure profiles will be used in order to examine the relationship of Mercier stability to that of high-n ballooing modes: a peaked profile[9] given by $P(\psi_N) = P_0(1-\psi_N)^2$, and a broad profile[6] given by $P(\psi_N) = P_0(1-\psi_N^2)^2$. Here $\psi_N = \psi/\psi_{edge}$ is the normalized toroidal flux, with $r_N = \sqrt{\psi_N}$ the normalized minor radius. Note that the peaked pressure profile is the profile that is normally used in stability calculations for the LHD[9], and that peaked pressure profiles similar to above one are observed in ordinary experiments in CHS[10].

Figure 1 shows the global rotational transform ι and the Mercier criterion parameter D_M as functions of ψ_N for both the peaked and broad pressure profiles with three different central β values. For the vacuum configuration considered here, the Shafranov shift is quite large, i.e., there is a substantial Pfirsch-Schlüter current. Consequently, ι and so the global magnetic shear s become highly deformed as β increases for both types of pressure profile. In particular, ι increases near the magnetic axis, but decreases near the periphery. Because a region of tokamak-like global magnetic shear appears near the magnetic axis and the stellarator-like magnetic shear is increased near the periphery, a shearless region occurs between them. As β increases, the global magnetic shear becomes very strong in the stellarator-like region near the plasma periphery.

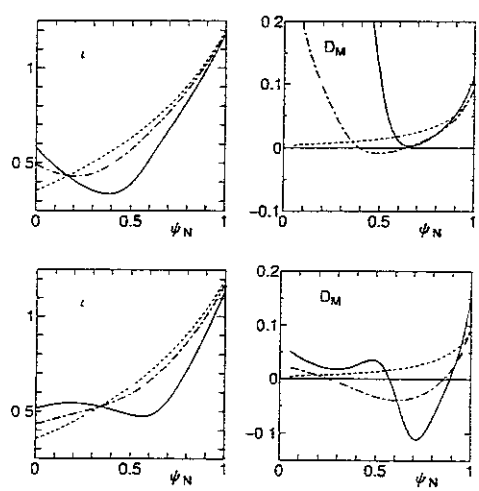

Fig. 1 : ι and D_M vs ψ_N: The upper (lower) graphs are for the peaked (broad) pressure profile. The dotted, dot-dashed, and solid curves correspond to $\beta_0 = 0, 4,$ and 8%, respectively. $D_M > 0$ implies Mercier stability.

3. LOCAL EQUILIBRIUM CHARACTERISTICS

A. Local magnetic shear

Equally spaced (ψ,θ) meshes in the Boozer coordinate system $(\psi,\ \theta,\ \zeta)$ for the peaked pressure profiles with three different central β values are shown in Fig. 2 on horizontally and vertically elongated poloidal cross sections.

In the field line coordinate system or covering space $(\psi,\ \eta,\ \alpha)$, which is related to the Boozer coordinate system $(\psi,\ \theta,\ \zeta)$ as $\eta = \theta,\quad \alpha = \zeta - \theta/\iota$ with α the label for the magnetic field lines, the local magnetic shear $\hat{s}$ can be expressed in terms of the global magnetic shear s and its oscillatory component $\tilde{s}$, as follows:

$$\hat{s} = s + \tilde{s},\quad s = \frac{2\psi}{\iota}\frac{d\iota}{d\psi},\quad \tilde{s} = \frac{\partial}{\partial\eta}\left\{\frac{2\psi g_{\psi\theta}}{g_{\theta\theta}}\right\},\quad \int^{\eta}\hat{s}d\eta = s(\eta-\theta_k) + \frac{2\psi g_{\psi\theta}}{g_{\theta\theta}}, \quad (1)$$

where $g_{ij} = \partial_i\vec{r}\cdot\partial_j\vec{r},\ (i,j = \psi,\theta,\zeta)$ and θ_k is the radial wave number. In the coordinate system used here, $\theta = 0$ or $\eta = 0$ corresponds to the outer side of the torus. Almost all the information about the local compression of the poloidal field appears in the behavior of the poloidal angle θ, as can be seen in Fig. 2. As the value of β_0 increases, there appears a *turning surface* (i.e., where $g_{\psi\theta} = 0$), which reflects the properties of the local magnetic shear through $\tilde{s}$. Near the magnetic axis, the global magnetic shear s is tokamak-like ($s < 0$) for the peaked pressure profile or very small ($s \sim 0$) for the broad pressure profile; this property can be seen in Fig. 1. Therefore, the local compression of the poloidal field increases radially outward in order to maintain toroidal force balance: $g_{\psi\theta} \sim c\sin\theta$ with $c > 0$, which leads to the situation with $s \lesssim 0$ and $\tilde{s} > 0$. In contrast, near the plasma periphery, ι exceeds unity and s is strongly stellarator-like ($s > 0$). The local compression of the poloidal field decreases radially outward, due to the large poloidal field on average: $g_{\psi\theta} \sim c\sin\theta$ with $c < 0$, which leads to the situation with $s > 0$ and $\tilde{s} < 0$. In both regions, $\hat{s}$ is reduced.

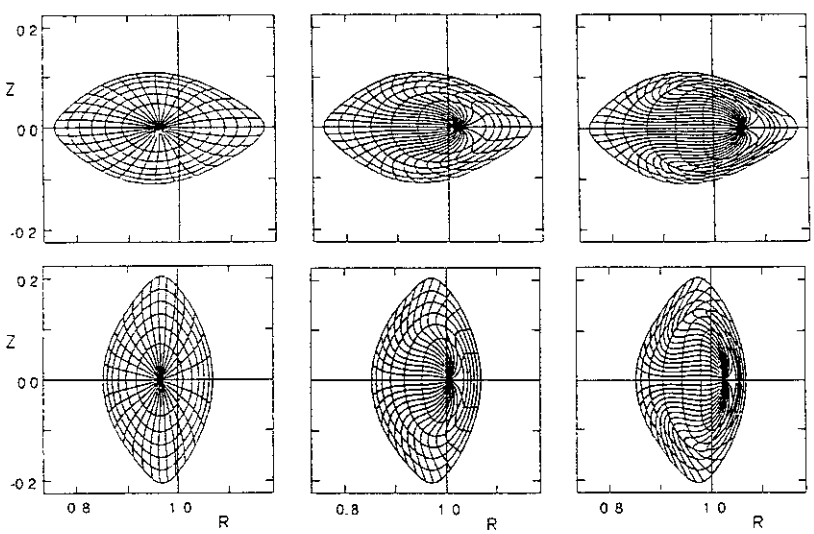

Fig. 2 : Equally spaced (ψ,θ) mesh in the Boozer coordinate system for $\beta_0 =$ 0%, 4%, and 8% from left-hand to right-hand graph.

The reduction of the stabilizing effect of the local magnetic shear in the region with stellarator-like global shear ($\psi_N = 0.56$) is exhibited in Fig. 3(a) for the peaked pressure profile with $\beta_0 = 8\%$, where the integrated local shear, $\left[\int^{\eta} \hat{s} d\eta\right]^2$, for $\theta_k = 0$, is plotted along a field line with $\alpha = 0$; on a horizontally elongated cross section, this field line passes through the outer midplane of the torus. For reference, the average integrated local shear $(s\eta)^2$ is also plotted in Fig. 3(a). We can understand that as β increases, the stabilizing effect of the local magnetic shear near $\eta = 0$ is significantly reduced. The vanishing of the (integrated) local magnetic shear at the outer side of the torus does not strongly depend on either the type of pressure profile or the magnetic field line label α, except that the critical β value at which the local magnetic shear vanishes does depend on the pressure profile.

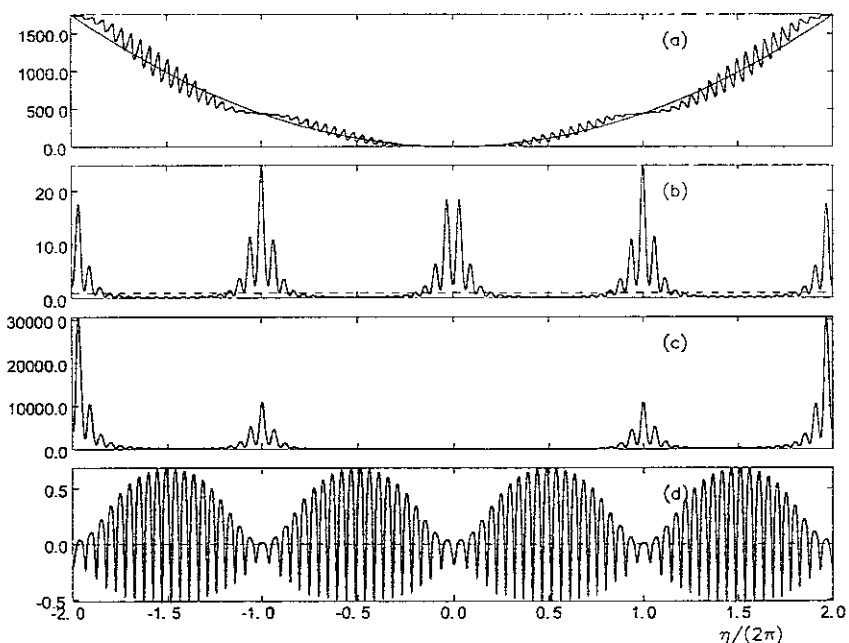

Fig. 3 : Variation along a magnetic field line of (a) $\left[\int^{\eta} \hat{s} d\eta\right]^2$*, with the reference* $(s\eta)^2$ *(thin curve); (b)* $|\nabla\psi|^2/(2\psi B_0)$*, with the reference* $|\nabla\psi|^2/(2\psi B_0) = 1$ *(thin dotted curve); (c)* $|\vec{k}_\perp|^2$*; and (d)* κ^n*. These quantities are shown at* $\psi_N = 0.56$*,* $\theta_k = 0$*, and* $\alpha = 0$ *for an equilibrium with a peaked pressure profile with* $\beta_0 = 8\%$*.*

B. Local shape of flux surfaces

At the outer side of the torus, the flux surfaces are locally compressed, because this is where the compression of the poloidal field varies radially. This situation is reflected in the local shape of the flux surfaces at the outer side of the torus, as expressed by $|\nabla\psi| = B\sqrt{g_{\theta\theta}}$. As shown in the poloidal cross sections with $\beta_0 = 8\%$ in Fig. 2, the variation of $|\nabla\psi|$ in the minor radius direction significantly changes across the *turning surface* on the outer side of the torus. At the outer side of the torus, adjacent flux surfaces become progressively nearer to

each other in radius as the *turning surface* is approached. In other words, the flux surfaces become more and more compressed. Once the *turning surface* is crossed, however, the flux surfaces become less compressed radially. The local compression of the flux surfaces at the outer side of the torus causes the flux surfaces to be locally uncompressed at the inner side of the torus due to toroidal flux conservation. Thus, the change of the local shape of a flux surface $|\nabla\psi|$ along a field line is quite noticeable as is shown in Fig. 3(b). Since it is caused by toroidal force balance (i.e., the Shafranov shift), the local compression or decompression of the flux surfaces becomes most noticeable as the value of β increases; however, it is independent of α, the magnetic field line label.

The variation of the local shape of the flux surfaces $|\nabla\psi|$ plays an important role in the stabilization of high-n ballooning modes for equilibria with large Shafranov shifts. The reason for this can be seen from the expression for the perpendicular wave number $|\vec{k}_\perp|$,

$$|\vec{k}_\perp|^2 = \frac{2\psi B^2}{B_0|\nabla\psi|^2} + \frac{|\nabla\psi|^2}{2\psi B_0}\left[\int^\eta \hat{s}d\eta\right]^2. \tag{2}$$

The secular stabilizing term $s(\eta-\theta_k)|\nabla\psi|$ is amplified through $|\nabla\psi|$ each time the field line transits the outer side of the torus, near $\eta = 2p\pi$ with p an integer, leading to an enhancement of its stabilizing effect. On the other hand, each time the field line transits the inner side of the torus, near $\eta = (2p+1)\pi$, the secular stabilizing term is diminished through $|\nabla\psi|$, leading to the reduction of its stabilizing effect. The characteristics of the local shape of the flux surfaces as expressed by $|\nabla\psi|$ are universal, at least for $L = 2$ heliotron/torsatron systems.

In Fig. 3(c), $|\vec{k}_\perp|^2$ is plotted along the same field line as that for Fig. 3(a). This graph shows that the field line bending stabilization effect on high-n ballooning modes is strongly modified as β is increased. Within one poloidal period along the field line ($|\eta| < \pi$), this stabilizing effect is significantly suppressed, both because the local shear associated with the poloidal field which is compressed at the outer side of the torus vanishes (Fig. 3(a)) and because the flux surfaces on the inner side of the torus are decompressed (Fig. 3(b)). On the other hand, this stabilizing effect is significantly enhanced farther out along the field line ($|\eta| \sim 2\pi$) due to the local compression of the flux surfaces at the outer side of the torus (Fig. 3(b)). This sort of modification is universal in $L = 2$ heliotron/torsatron systems with a large Shafranov shift and is almost independent of both the magnetic field line label and the pressure profile, except for the β value at which the modification becomes significant.

C. Local magnetic curvature

The local magnetic curvature in heliotron/torsatron systems consists of two components. One component is due to toroidicity, just as in a tokamak plasma. This mainly comes from the vacuum toroidal field and hence has no dependence on α. The other component is due to helicity (i.e., of the helical coils),

which mainly arises from the saddle-like profile for the magnetic field strength, reflecting that in a straight helix. On every poloidal cross section, the outside of the torus corresponds to locally "bad" magnetic curvature, and the inside to "good" curvature, in terms of the toroidicity contribution. In terms of the helicity contribution, however, the regions between the helical coils correspond to the locally bad magnetic curvature in each poloidal cross section, and the regions under the helical coils to locally good curvature. The variation of the magnetic field strength due to the helicity is comparable with that due to the toroidicity. Therefore, the local magnetic curvature is worst at the outer side of the torus in a horizontally elongated poloidal cross section (cf. upper graphs in Fig. 2). At the outer side of the torus in a vertically elongated poloidal cross section (cf. lower graphs in Fig. 2), the locally bad magnetic curvature due to the toroidicity is canceled by the locally good magnetic curvature due to the helicity. Thus, the local magnetic curvature at the outer side of the torus strongly depends on α, the label of the magnetic field line in the covering space (ψ, η, α). This situation is completely different from that in a tokamak plasma. In a tokamak plasma, the local magnetic curvature is independent of the field line label α because of the toroidal symmetry.

In Fig. 3(d), the contravariant normal magnetic curvature $\kappa^n = 2\psi\vec{\kappa}\cdot\nabla\psi/|\nabla\psi|^2$ is plotted along the magnetic field line. The phase due to the toroidicity and that due to the helicity are both quite evident. At the outer side of the torus, where $\eta = 2p\pi$ with p an integer, locally unfavorable magnetic curvature occurs near $\eta = 0$ and $\pm 4\pi$, but locally favorable curvature at $\eta = \pm 2\pi$. Because of such behavior, the local magnetic curvature is expected to have a strong dependence on the magnetic field line (i.e., on α). This sort of strong magnetic field line dependence (α-dependence) of the local magnetic curvature is a universal feature in heliotron/torsatron systems with appreciable helical ripple.

4. STABILITY PROPERTIES

Pressure profiles have a strong influence on high-n ballooning modes through the Mercier criterion. The broad pressure profiles create the highly Mercier unstable equilibria with the maximum pressure gradient within the Mercier unstable region. In such equilibria, the high-n ballooning modes are easily destabilized at a relatively low-β value, which leads to the situation that high-n ballooning modes become unstable before the stabilizing effects within (near) one poloidal period along the field line are suppressed (enhanced) enough by the Shafranov shift. Thus, high-n modes have a tendency to have an extended interchange-like structure along the magnetic field line. The high-n modes occuring near a flux surface giving the marginal stability have the extended interchange-like structure as is shown in Fig. 4(a). The extended structure so relaxes the α-dependence of the destabilizing term that near the marginal stability high-n modes become tokamak-like modes with the eigenvalue $\omega^2 \sim \omega^2(\psi, \theta_k)$. Away from the flux

surface giving the marginal stability, high-n modes have fairly localized structure that α-dependence of ω^2 becomes strong. Thus, in (ψ, θ_k, α) space, the spheroidal level surfaces of ω^2 of localized modes are surrounded with the cylindorical level surfaces of ω^2 of extended modes. Although the growth rates of those tokamak-like extended modes are small, those are dangerous since those may lead to low-n modes.[6]

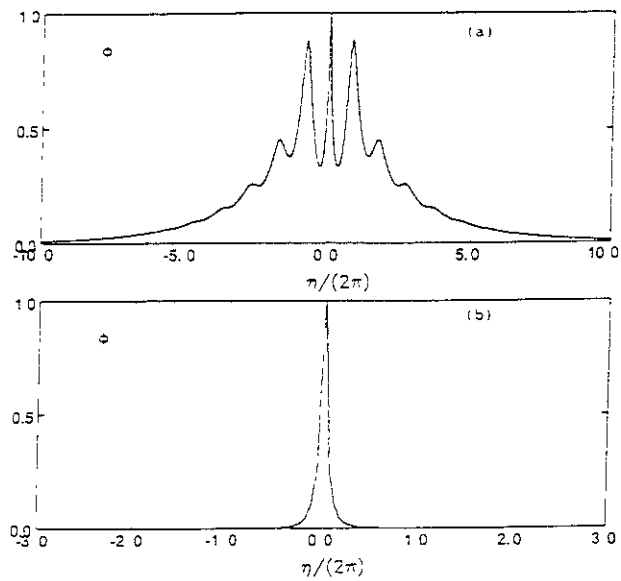

Fig. 4 : High-n ballooning mode eigenfunction (a) $\Phi(\psi_N = 0.39, \theta_k = 0, \alpha = 0)$ *for a strongly Mercier-unstable equilibrium with the broad pressure profile with* $\beta_0 = 4\%$ *and (b)* $\Phi(\psi_N = 0.56, \theta_k = 0, \alpha = 0)$ *for a completely Mercier-stable equilibrium with the peaked pressure profile with* $\beta_0 = 8\%$.

In contrast to it, in the slightly Mercier unstable or completely Mercier stable equilibria, created by the peaked pressure profiles usually used in standard stability analyses[9] and obtained in ordinal CHS experiments[10], the high-n ballooning modes are destabilized after the stabilizing effects within (near) one poloidal period along the magnetic field line are suppressed (enhanced) enough by the Shafranov shift. Thus, these modes are highly localized within one poloidal period as is shown in Fig. 4(b), which leads to such a strong α-dependence of the eigenvalues that the level surfaces of $\omega^2(\psi, \theta_k, \alpha)$ (≤ 0) become topologically spheroid in (ψ, θ_k, α) space as shown in Fig. 5. The area indicated by the thick closed curves corresponds to the contours for the negative eigenvalues of high-n ballooning modes, and the area indicated by the thin unclosed curves to the contours for the positive eigenvalues of high-n TAE modes. Note that the unstable region in θ_k is very narrow. Those highly localized modes with the spheroidal level surfaces of ω^2 never lead to the low-n modes and are inherent to three-dimensional equlibria. Note that the tokamak-like modes leading to low-n modes appear only near the marginal stability in highly Mercier unstable equilibria. Although those inherent high-n modes with the spheroidal level surfaces of ω^2 may be considered to give β-limit to completely Mercier

stable equilibria, we should notice that those modes are considered to be so highly localized in each toroidal pitch of the helical coils in the configuration space that the expected toroidal mode numbers n would be quite large, i.e., $n \sim n_{min}, n_{min}+M, n_{min}+2M, n_{min}+3M, \cdots$, where n_{min} is at least the order of M. Therefore, in order to evaluate the β-limit due to these high-n modes inherent to three-dimensional equilibria, kinetic effects due to an ion diamagnetic frequency and Finite Larmor Radius stabilizing effects must be evaluated along with them. Such kinetic effects on these high-n modes inherent to three-dimensional equilibria and the relation to ones in other devices will be addressed.

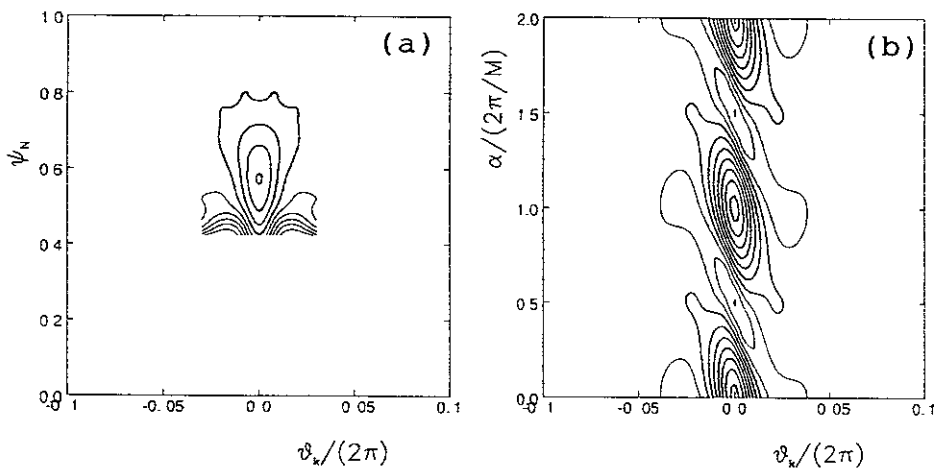

Fig. 5 : (a) The θ_k and ψ-dependence of Ω^2, with $\alpha = 0$, and (b) the θ_k and α-dependence of the most unstable Ω^2, with $\psi_N = 0.56$, both for the peaked pressure profile with $\beta_0 = 8\%$.

ACKNOWLEDGMENTS

The authors acknowledge to Prof. A. Iiyoshi and Prof. T. Sato for continuous encouragement.

REFERENCES

[1] SHAFRANOV, V. D., Phys. Fluids **26** (1983) 357.
[2] COOPER, W. A., *et al.*, Nucl. Fusion **29** (1989) 617.
[3] LYON, J. F., *et al.*, Fusion Technol. **10** (1986) 179.
[4] DEWAR, R. L. and GLASSER, A. H., Phys. Fluids **26** (1983) 3038.
[5] IIYOSHI, A., *et al.*, Fusion Technol. **17** (1990) 148.
[6] COOPER, W. A., *et al.*, Phys. Plasmas **3** (1996) 275.
[7] HAZELTINE, R. D. and MEISS, J. D., Phys.Reports **121** (1985) 1.
[8] HIRSHMAN, S. P., Phys. Fluids **26** (1983) 3553.
[9] ICHIGUCHI, K, *et al.*, Nucl. Fusion **33** (1993) 481.
[10] OKAMURA, S., *et al.*, Nucl. Fusion **35** (1995) 283.

Recent Issues of NIFS Series

NIFS-416 M. Iwase, K. Ohkubo, S. Kubo and H. Idei
Band Rejection Filter for Measurement of Electron Cyclotron Emission during Electron Cyclotron Heating; May 1996

NIFS-417 T. Yabe, H. Daido,T. Aoki, E. Matsunaga and K. Arisawa,
Anomalous Crater Formation in Pulsed-Laser-Illuminated Aluminum Slab and Debris Distribution; May 1996

NIFS-418 J. Uramoto,
Extraction of K^- Mesonlike Particles from a D_2 Gas Discharge Plasma in Magnetic Field; May 1996

NIFS-419 J. Xu, K. Toi, H. Kuramoto, A. Nishizawa, J. Fujita, A. Ejiri, K. Narihara, T. Seki, H. Sakakita, K. Kawahata, K. Ida, K. Adachi, R. Akiyama, Y. Hamada, S. Hirokura, Y. Kawasumi, M. Kojima, I. Nomura, S. Ohdachi, K.N. Sato
Measurement of Internal Magnetic Field with Motional Stark Polarimetry in Current Ramp-Up Experiments of JIPP T-IIU; June 1996

NIFS-420 Y.N. Nejoh,
Arbitrary Amplitude Ion-acoustic Waves in a Relativistic Electron-beam Plasma System; July 1996

NIFS-421 K. Kondo, K. Ida, C. Christou, V.Yu.Sergeev, K.V.Khlopenkov, S.Sudo, F. Sano, H. Zushi, T. Mizuuchi, S. Besshou, H. Okada, K. Nagasaki, K. Sakamoto, Y. Kurimoto, H. Funaba, T. Hamada, T. Kinoshita, S. Kado, Y. Kanda, T. Okamoto, M. Wakatani and T. Obiki,
Behavior of Pellet Injected Li Ions into Heliotron E Plasmas; July 1996

NIFS-422 Y. Kondoh, M. Yamaguchi and K. Yokozuka,
Simulations of Toroidal Current Drive without External Magnetic Helicity Injection; July 1996

NIFS-423 Joong-San Koog,
Development of an Imaging VUV Monochromator in Normal Incidence Region: July 1996

NIFS-424 K. Orito,
A New Technique Based on the Transformation of Variables for Nonlinear Drift and Rossby Vortices; July 1996

NIFS-425 A. Fujisawa, H. Iguchi, S. Lee, T.P. Crowley, Y. Hamada, H. Sanuki, K. Itoh, S. Kubo, H. Idei, T. Minami, K. Tanaka, K. Ida, S. Nishimura, S. Hidekuma, M. Kojima, C. Takahashi, S. Okamura and K. Matsuoka,
Direct Observation of Potential Profiles with a 200keV Heavy Ion Beam Probe and Evaluation of Loss Cone Structure in Toroidal Helical Plasmas on

the Compact Helical System; July 1996

NIFS-426 H. Kitauchi, K. Araki and S. Kida,
Flow Structure of Thermal Convection in a Rotating Spherical Shell; July 1996

NIFS-427 S. Kida and S. Goto,
Lagrangian Direct-interaction Approximation for Homogeneous Isotropic Turbulence; July 1996

NIFS-428 V.Yu. Sergeev, K.V. Khlopenkov, B.V. Kuteev, S. Sudo, K. Kondo, F. Sano, H. Zushi, H. Okada, S. Besshou, T. Mizuuchi, K. Nagasaki, Y. Kurimoto and T. Obiki,
Recent Experiments on Li Pellet Injection into Heliotron E; Aug. 1996

NIFS-429 N. Noda, V. Philipps and R. Neu,
A Review of Recent Experiments on W and High Z Materials as Plasma-Facing Components in Magnetic Fusion Devices; Aug. 1996

NIFS-430 R.L. Tobler, A. Nishimura and J. Yamamoto,
Design-Relevant Mechanical Properties of 316-Type Stainless Steels for Superconducting Magnets; Aug. 1996

NIFS-431 K. Tsuzuki, M. Natsir, N. Inoue, A. Sagara, N. Noda, O. Motojima, T. Mochizuki, T. Hino and T. Yamashina,
Hydrogen Absorption Behavior into Boron Films by Glow Discharges in Hydrogen and Helium; Aug. 1996

NIFS-432 T.-H. Watanabe, T. Sato and T. Hayashi,
Magnetohydrodynamic Simulation on Co- and Counter-helicity Merging of Spheromaks and Driven Magnetic Reconnection; Aug. 1996

NIFS-433 R. Horiuchi and T. Sato,
Particle Simulation Study of Collisionless Driven Reconnection in a Sheared Magnetic Field; Aug. 1996

NIFS-434 Y. Suzuki, K. Kusano and K. Nishikawa,
Three-Dimensional Simulation Study of the Magnetohydrodynamic Relaxation Process in the Solar Corona. II.; Aug. 1996

NIFS-435 H. Sugama and W. Horton,
Transport Processes and Entropy Production in Toroidally Rotating Plasmas with Electrostatic Turbulence; Aug. 1996

NIFS-436 T. Kato, E. Rachlew-Källne, P. Hörling and K.-D Zastrow,
Observations and Modelling of Line Intensity Ratios of OV Multiplet Lines for 2s3s 3S1 - 2s3p 3Pj; Aug. 1996

NIFS-437 T. Morisaki, A. Komori, R. Akiyama, H. Idei, H. Iguchi, N. Inoue, Y. Kawai, S.

Kubo, S. Masuzaki, K. Matsuoka, T. Minami, S. Morita, N. Noda, N. Ohyabu, S. Okamura, M. Osakabe, H. Suzuki, K. Tanaka, C. Takahashi, H. Yamada, I. Yamada and O. Motojima,
Experimental Study of Edge Plasma Structure in Various Discharges on Compact Helical System; Aug. 1996

NIFS-438 A. Komori, N. Ohyabu, S. Masuzaki, T. Morisaki, H. Suzuki, C. Takahashi, S. Sakakibara, K. Watanabe, T. Watanabe, T. Minami, S. Morita, K. Tanaka, S. Ohdachi, S. Kubo, N. Inoue, H. Yamada, K. Nishimura, S. Okamura, K. Matsuoka, O. Motojima, M. Fujiwara, A. Iiyoshi, C. C. Klepper, J.F. Lyon, A.C. England, D.E. Greenwood, D.K. Lee, D.R. Overbey, J.A. Rome, D.E. Schechter and C.T. Wilson,
Edge Plasma Control by a Local Island Divertor in the Compact Helical System; Sep. 1996 (IAEA-CN-64/C1-2)

NIFS-439 K. Ida, K. Kondo, K. Nagaski T. Hamada, H. Zushi, S. Hidekuma, F. Sano, T. Mizuuchi, H. Okada, S. Besshou, H. Funaba, Y. Kurimoto, K. Watanabe and T. Obiki,
Dynamics of Ion Temperature in Heliotron-E; Sep. 1996 (IAEA-CN-64/CP-5)

NIFS-440 S. Morita, H. Idei, H. Iguchi, S. Kubo, K. Matsuoka, T. Minami, S. Okamura, T. Ozaki, K. Tanaka, K. Toi, R. Akiyama, A. Ejiri, A. Fujisawa, M. Fujiwara, M. Goto, K. Ida, N. Inoue, A. Komori, R. Kumazawa, S. Masuzaki, T. Morisaki, S. Muto, K. Narihara, K. Nishimura, I. Nomura, S. Ohdachi, M.. Osakabe, A. Sagara, Y. Shirai, H. Suzuki, C. Takahashi, K. Tsumori, T. Watari, H. Yamada and I. Yamada,
A Study on Density Profile and Density Limit of NBI Plasmas in CHS; Sep. 1996 (IAEA-CN-64/CP-3)

NIFS-441 O. Kaneko, Y. Takeiri, K. Tsumori, Y. Oka, M. Osakabe, R. Akiyama, T. Kawamoto, E. Asano and T. Kuroda,
Development of Negative-Ion-Based Neutral Beam Injector for the Large Helical Device; Sep. 1996 (IAEA-CN-64/GP-9)

NIFS-442 K. Toi, K.N. Sato, Y. Hamada, S. Ohdachi, H. Sakakita, A. Nishizawa, A. Ejiri, K. Narihara, H. Kuramoto, Y. Kawasumi, S. Kubo, T. Seki, K. Kitachi, J. Xu, K. Ida, K. Kawahata, I. Nomura, K. Adachi, R. Akiyama, A. Fujisawa, J. Fujita, N. Hiraki, S. Hidekuma, S. Hirokura, H. Idei, T. Ido, H. Iguchi, K. Iwasaki, M. Isobe, O. Kaneko, Y. Kano, M. Kojima, J. Koog, R. Kumazawa, T. Kuroda, J. Li, R. Liang, T. Minami, S. Morita, K. Ohkubo, Y. Oka, S. Okajima, M. Osakabe, Y. Sakawa, M. Sasao, K. Sato, T. Shimpo, T. Shoji, H. Sugai, T. Watari, I. Yamada and K. Yamauti,
Studies of Perturbative Plasma Transport, Ice Pellet Ablation and Sawtooth Phenomena in the JIPP T-IIU Tokamak; Sep. 1996 (IAEA-CN-64/A6-5)

NIFS-443 Y. Todo, T. Sato and The Complexity Simulation Group,
Vlasov-MHD and Particle-MHD Simulations of the Toroidal Alfvén Eigenmode; Sep. 1996 (IAEA-CN-64/D2-3)

NIFS-444 A. Fujisawa, S. Kubo, H. Iguchi, H. Idei, T. Minami, H. Sanuki, K. Itoh, S. Okamura, K. Matsuoka, K. Tanaka, S. Lee, M. Kojima, T.P. Crowley, Y. Hamada, M. Iwase, H. Nagasaki, H. Suzuki, N. Inoue, R. Akiyama, M. Osakabe, S. Morita, C. Takahashi, S. Muto, A. Ejiri, K. Ida, S. Nishimura, K. Narihara, I. Yamada, K. Toi, S. Ohdachi, T. Ozaki, A. Komori, K. Nishimura, S. Hidekuma, K. Ohkubo, D.A. Rasmussen, J.B. Wilgen, M. Murakami, T. Watari and M. Fujiwara,
An Experimental Study of Plasma Confinement and Heating Efficiency through the Potential Profile Measurements with a Heavy Ion Beam Probe in the Compact Helical System; Sep. 1996 (IAEA-CN-64/C1-5)

NIFS-445 O. Motojima, N. Yanagi, S. Imagawa, K. Takahata, S. Yamada, A. Iwamoto, H. Chikaraishi, S. Kitagawa, R. Maekawa, S. Masuzaki, T. Mito, T. Morisaki, A. Nishimura, S. Sakakibara, S. Satoh, T. Satow, H. Tamura, S. Tanahashi, K. Watanabe, S. Yamaguchi, J. Yamamoto, M.Fujiwara and A. Iiyoshi,
Superconducting Magnet Design and Construction of LHD; Sep. 1996 (IAEA-CN-64/G2-4)

NIFS-446 S. Murakami, N. Nakajima, S. Okamura, M. Okamoto and U. Gasparino,
Orbit Effects of Energetic Particles on the Reachable β–Value and the Radial Electric Field in NBI and ECR Heated Heliotron Plasmas; Sep. 1996 (IAEA-CN-64/CP -6) Sep. 1996

NIFS-447 K. Yamazaki, A. Sagara, O. Motojima, M. Fujiwara, T. Amano, H. Chikaraishi, S. Imagawa, T. Muroga, N. Noda, N. Ohyabu, T. Satow, J.F. Wang, K.Y. Watanabe, J. Yamamoto , H. Yamanishi, A. Kohyama, H. Matsui, O. Mitarai, T. Noda, A.A. Shishkin, S. Tanaka and T. Terai
Design Assessment of Heliotron Reactor; Sep. 1996 (IAEA-CN-64/G1-5)

NIFS-448 M. Ozaki, T. Sato and the Complexity Simulation Group,
Interactions of Convecting Magnetic Loops and Arcades; Sep. 1996

NIFS-449 T. Aoki,
Interpolated Differential Operator (IDO) Scheme for Solving Partial Differential Equations; Sep. 1996

NIFS-450 D. Biskamp and T. Sato,
Partial Reconnection in the Sawtooth Collapse; Sep. 1996

NIFS-451 J. Li, X. Gong, L. Luo, F.X. Yin, N. Noda, B. Wan, W. Xu, X. Gao, F. Yin, J.G. Jiang, Z. Wu., J.Y. Zhao, M. Wu, S. Liu and Y. Han,
Effects of High Z Probe on Plasma Behavior in HT-6M Tokamak; Sep. 1996

NIFS-452 N. Nakajima, K. Ichiguchi, M. Okamoto and R.L. Dewar,
Ballooning Modes in Heliotrons/Torsatrons; Sep. 1996